1C12

Photofragment Imaging Apparatus for Measuring Momentum Distributions in Dissociative Photoionization of Fullerenes

[*] *Department of Structural Molecular Science, Graduate University for Advance Studies, Myodaiji, Okazaki, 444-8585, Japan*

[¶]Institute for Molecular Science, Myodaiji, Okazaki, 444-8585, Japan

○ Bhim P. Kafle[*], Md. S. I. Prodhan[*], Hideki Katayanagi[*¶], and Koichiro Mitsuke[*¶]

The yield curves of the fragments C_{60-2n}^{z+} and C_{70-2n}^{z+} ($n \geq 1$, $z \geq 1$) produced by photoionization of solitary fullerenes of C_{60} and $C_{70,}$ respectively, have been reported in the range of 45-150 eV [1,2].Comparison between the experimental results and observation from theoretical studies revealed that the excess energy is statistically distributed among the internal degrees of freedom of the parent ions and C_2 units are ejected sequentially:

$$C_{60}^{+} \rightarrow C_{58}^{+} + C_2,\ C_{58}^{+} \rightarrow C_{56}^{+} + C_2,\ \ldots\ C_{60-2n+2}^{z+} \rightarrow C_{60-2n}^{+} + C_2. \qquad (1)$$

Moreover, it is assumed that there exists no potential barrier along the reaction coordinate and that no resonant state participates during dissociation. To clarify the above argument, we have developed a photofragment imaging apparatus based on time-of-flight (TOF) mass spectrometry to measure the kinetic energy and angular distributions of the fragments.

There are only a few experimental studies of product analysis of the fragments. Translational energy distribution of C_{60-2n}^{+} have been measured by several groups to gain insight into the energetics and fragmentation mechanism. Hertel and coworkers [3] evaluated the kinetic energies of C_{60-2n}^{+} ($1 \leq n \leq 14$) produced by photoionization of C_{60}^{+}. Later Märk and co-workers [4] fulfilled electron impact ionization of C_{60} and reported a value of ca. 0.45 eV as the total average kinetic energy release in the decomposition of C_{60}^{+} into C_{60-2n}^{+} ($1 \leq n \leq 8$).These authors suggested that not only sequential C_2 ejection of process (1) but also single-step two-fragment fission of the parent C_{60}^{+} ions

$$C_{60}^{+} \rightarrow C_{60-2n}^{+} + C_{2n}. \qquad (2)$$

are possible mechanisms for the formation of C_{60-2n}^{+}.

In the present study, we will develop a new version of momentum imaging spectrometer to obtain reliable velocity distributions of the fullerene fragments. From photofragment images, we will be able to decide on which mechanism dominates fragmentation of fullerene ions, since three-dimensional velocity distributions are expected to considerably differ for different mechanisms. Moreover, closer inspection of the images may allow us to directly probe the properties of transition states correlated to the dissociation channels. If dissociation channels involve passage over an exit barrier, the translational energy distribution makes a peak at some fraction of the barrier height. In contrast, if little or no exit barrier exists on dissociation channels, the distribution shows a peak at close or equal to zero because energy partitioning occurs statistically among all the internal degrees of freedom of the parent species.

We adopted the Eppink–Parker type three-element velocity focusing lens system (electrodes R,E, and T) [5] to achieve the kinetic energy resolution of ca. 0.01 eV on the photofragment images. Furthermore, to select a bunch of fragments having the same mass-to-charge ratio m/z from neighboring bunches (m±24)/z, for example, to separate C_{58}^{+} from C_{60}^{+} and C_{56}^{+}, we utilized a potential switcheable mass gate M and an ion reflector G, which are kept very close to the imaging detector (PSD) inside the TOF tube, as demonstrated in Fig. 1.

The operating principle of these two components of the spectrometer is as follows: As long as the tube of the mass gate is kept grounded, all fragments are reflected back by the ion reflector and do not impinge against the PSD. In contrast, when an entire bunch of the fragments having an expected m/z arrives inside the mass gate, a pulsed voltage is applied there. The potential energies of the ions in this bunch are suddenly elevated, so that only these ions can pass through the ion reflector and reach the PSD.

For optimizing the dimensions of the setup, we performed ion trajectory simulations utilizing the SIMION software [6]. We considered that the dissociative ionization of C_{60} takes place within a region of rectangular parallelepiped $\Delta x \Delta y \Delta z = 1 \times 3 \times 1$ mm^3 in the ionization region of the spectrometer. The y-coordinate of this region ranges from -1.5 to +1.5 mm because the y-direction is assigned to the passage of synchrotron radiation as shown in the Fig. 1 (the x-direction represents the TOF axis). In ion trajectory simulations the eight corners and the center of the ionization region were chosen for the starting points of the trajectories. From each point

171 trajectories were generated in the elevation angle range of – 90° to + 90° at intervals of 22.5 ° and in the azimuth angle range of 0° to + 180° at intervals of 10°. The amplitude and duration of the pulsed voltage applied to repeller were 300 V and 7 μs, respectively, and the rising edge of this pulse preceded that of the pulsed voltage applied to the mass gate by 44.5 μs. The amplitude and duration of the pulsed voltage applied to the mass gate were set to 120 V and 1 μs, respectively. The ratio of voltages between that applied to extractor and that to repeller was set to be constant at 0.714, while a continuous voltage of 320 V was applied to the central electrode of the ion reflector.

With the above parameters, the simulated trajectories of C_{60}^+, C_{58}^+ and C_{56}^+ at initial kinetic energy of 0.1 eV show that the trajectories of both unwanted ions C_{60}^+ and C_{56}^+ are reflected completely. On the other hand, most of the trajectories of C_{58}^+, the ion whose momentum image we wish to measure, are found to go beyond the ion reflector and reach the PSD. This observation provides direct evidence for exclusive imaging detection of C_{58}^+ after excluding C_{60}^+ and C_{56}^+ with the same kinetic energies.

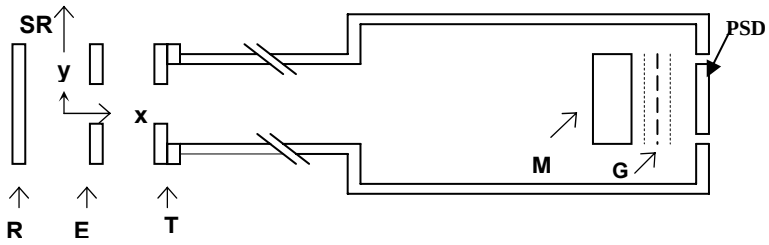

Figure 1. Schematic view of the momentum imaging spectrometer in combination with the mass gate M and ion reflector G. The dimensions of all the electrodes are optimized by using the SIMION 3D software. R, Repeller; E, extractor; T, Entrance electrode of a drift tube; SR, synchrotron radiation.

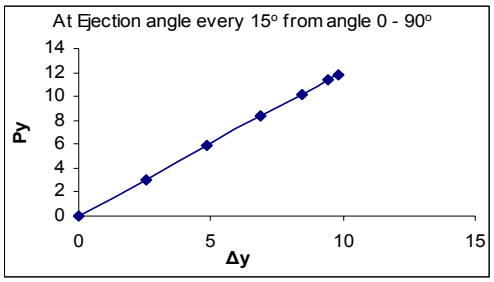

Figure 2. Quasi-linear relationship between the y-component of the momentum and that of the displacement at PSD.

Moreover, a quasi-linearship between the y-component of the momentum (Py) and that of the displacement at PSD (Δy) shows linear trend (Fig. 2), which allows us to translate the displacement of ionic fragment on PSD to velocity and angular distribution of a desired fragment.

Figure 3 shows the image of C_{58}^+ ions on the PSD at the kinetic energies of 0.1eV (triangles) and 0.11eV (circles). We took into account the ion trajectories generated in the elevation and azimuth angle ranges of 0° to + 90° and 0° to + 180°, respectively, which cover only one quarter of the full three-dimensional trajectories over the 4π solid angle. The trajectories with a given elevation angle form a horizontal stripe, and the envelope of all the stripes makes an arc, which clearly demonstrates that scattering distribution in spherical symmetry can be successfully projected on an image plane. It is likely that C_{58}^+ fragment ions with kinetic energy difference of 0.01 eV are almost separable. Comparison between the simulations with and without the ion reflector confirmed that the images are not distorted in the presence of the ion reflector. The present momentum imaging spectrometer will be constructed and installed in the end station of beam line 2B in the UVSOR facility.

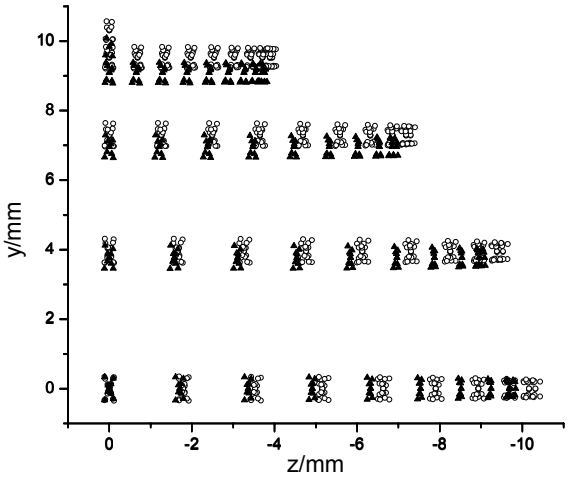

Figure 3. Projection of the three-dimensional scattering distribution of C_{58}^+ ions on the PSD at the initial kinetic energies of 0.1 (▲) and 0.11 eV (O).

REFERENCES

1. J. Kou, T. Mori, Y. Kubozono, and K. Mitsuke, Phys. Chem. Chem. Phys. **7**, 119-123 (2005).
2. K. Mitsuke, H. Katayanagi, J. Kou, T. Mori and Y. Kubozono, Am. Inst. Phys. CP **811**, 161-166 (2006).
3. H. Gaber, R. Hiss, H. G. Busmann, and I. V. Hertel, Z. Phys. D **24**, 307-309 (1992).
4. D. Muigg, G. Denifl, P. Scheier, K. Becker, and T. D. Mark, J. Chem. Phys. **108**, 963-970 (1998).
5. A. T. J. B. Eppink and D. H. Parker, Rev. Sci. Instrum. **68**, 3477-3484 (1997).
6. D. A. Dahl, SIMION 3D Version 7.0 User's Manual, Idaho falls: 2000.